Sensing and Reconstruction of 3D Deformation on Pneumatic Soft Robots

Scharff, Rob B.N.; Fang, Guoxin; Tian, Yingjun; Wu, Jun; Geraedts, J. M.P.; Wang, Charlie C.L.

DOI
10.1109/TMECH.2021.3078263

Publication date
2021

Document Version
Final published version

Published in
IEEE/ASME Transactions on Mechatronics

Citation (APA)
Scharff, R. B. N., Fang, G., Tian, Y., Wu, J., Geraedts, J. M. P., & Wang, C. C. L. (2021). Sensing and Reconstruction of 3D Deformation on Pneumatic Soft Robots. *IEEE/ASME Transactions on Mechatronics*, *26*(4), 1877-1885. Article 9426391. https://doi.org/10.1109/TMECH.2021.3078263

Sensing and Reconstruction of 3D Deformation on Pneumatic Soft Robots

Rob B.N. Scharff, *Student Member, IEEE,* Guoxin Fang, *Student Member, IEEE,* Yingjun Tian, Jun Wu, Jo M.P. Geraedts, and Charlie C.L. Wang†, *Senior Member, IEEE*

***Abstract*—Real-time proprioception is a challenging problem for soft robots, which have virtually infinite degrees-of-freedom in body deformation. When multiple actuators are used, it becomes more difficult as deformation can also occur on actuators caused by interaction between each other. To tackle this problem, we present a method in this paper to sense and reconstruct 3D deformation on pneumatic soft robots by first integrating multiple low-cost sensors inside the chambers of pneumatic actuators and then using machine learning to convert the captured signals into shape parameters of soft robots. An exterior motion capture system is employed to generate the datasets for both training and testing. With the help of good shape parameterization, the 3D shape of a soft robot can be accurately reconstructed from signals obtained from multiple sensors. We demonstrate the effectiveness of this approach on two soft robot designs – a robotic joint and a deformable membrane. After parameterizing the deformation of these soft robots into compact shape parameters, we can effectively train the neural networks to reconstruct the 3D deformation from the sensor signals. The sensing and shape prediction pipeline can run at 50Hz in real-time on a consumer-level device.**

***Index Terms*—Proprioception, 3D Deformation, Pneumatic Actuators, Soft Robotics**

I. Introduction

Proprioception for soft robots is a challenging problem because of the virtually infinite degrees of freedom (DOFs) of the deformable bodies, and because there is no off-the-shelf sensor available. However, accurate proprioception is crucial for closing the loop of control. Existing solutions generally conduct a simplified model according to a specific soft robot design – e.g., sensing a single bending angle [1] or curvature [2]. A general and easy-to-fabricate solution for sensing 3D deformation is needed. In this paper, we propose a method using low-cost sensors to realize accurate proprioception and real-time 3D shape reconstruction. Our approach is based on a data-driven strategy that can be generally applied to different designs based on their own shape parameterization.

A. Related Work

The literature is reviewed from three angles, namely sensors, deformation acquisition and machine learning.

R.B.N. Scharff is with the Bioinspired Soft Robotics Laboratory, Istituto Italiano di Tecnologia (IIT), Italy

R.B.N. Scharff, G. Fang, J. Wu, and J.M.P. Geraedts are with the Faculty of Industrial Design Engineering, Delft University of Technology (TU Delft), The Netherlands.

G. Fang, Y. Tian and C.C.L. Wang are with the Department of Mechanical, Aerospace and Civil Engineering, The University of Manchester, UK

†Corresponding Author: changling.wang@manchester.ac.uk

Revision prepared on March 15th, 2021.

1) Sensors for proprioception: A large variety of sensors have been developed for proprioception in soft robotics. For soft bending actuators, proprioceptive sensing is commonly achieved by embedding paths of conductive materials that change their resistivity upon deformation, such as liquid metal [3], a 3D-printed carbon black/PLA compound [4], [5], commercial flex sensors based on conductive ink [1], conductive ionogel [6], PDMS impregnated with carbon nanotubes [7], or laser-cut patterns from off-the-shelf conductive silicone [8]. Proprioception can also be achieved by magnetic sensing [9] and inductance-based sensing [10]. The inductance-based sensing method can also be applied to a continuum joint [11]. However, most of the sensors mentioned above cannot accommodate very large strains or cannot capture multiple DOFs, making them unsuitable for other types of actuators, such as elongational actuators or three-dimensionally deforming surfaces. Moreover, integrating these sensors into an actuator is usually cumbersome during fabrication.

The use of optical sensing for proprioception in soft robots has been shown to have great potential. Examples of optical sensing for soft robots include the stretchable optical waveguides for use in bending actuators [2], [12], macrobend optical sensing for elongational actuators [13], optical distance sensors on a helical flexible printed circuit board for a soft robotic joint [14], fiber optics in a three-dimensionally deforming surface [15], the use of fluidic channels in combination with an external camera [16], and embedded cameras for tactile sensing [17], [18], [19] and inflatable bellows [20]. However, some of these approaches can only sense relatively simple deformation (e.g., it is difficult to embed optical waveguides and fluidic channels inside three-dimensionally deforming surfaces or elongational actuators). Furthermore, the image-texture-based methods can only be used in large actuators because of the size of cameras.

In previous work, we demonstrated that accurate proprioception of soft robots could be achieved by integrating a light source, color sensors (photodiodes) and color patterns inside the air chambers of pneumatic bending actuators [21], [22]. Deformation of the air chamber changes the reflection and traveling distance of the light coming from the light source(s), which lead to changes in the light intensity and the colors observed by the optical sensors. A similar principle was applied for a linear bellow by using only four phototransistors [23]. Following the same working principle, we demonstrate in this paper that accurate proprioception of three-dimensionally deformed soft robots can be realized by using only light-dependent resistors (LDRs) and light-emitting diodes (LEDs).

In contrast to existing solutions, this solution can be easily integrated into many different types of soft pneumatic actuators while achieving highly accurate proprioception for soft robots interacting with their environment.

2) Deformation acquisition: An important challenge in sensing soft robot deformation is how to obtain accurate ground truth information in deformation. Simplified information has been sensed in prior research, including the bending angle [1], the curvature [2] and the position of the tip point [24], [25]. However, important information on the shape of a soft robot is lost. A straightforward solution is to increase the number of sensed points on the actuator. However, the number of points is limited when physical manipulators [25] or sensors (e.g., inertial measurement units [11] or electromagnetic sensors [13], [26]) are used to determine the position of each point. For these reasons, systems that capture markers on a soft robot with one or more camera sensors are a popular choice for capturing ground truth information of soft objects (ref. [11], [15], [22], [27], [28]). The captured marker coordinates on the robot can be used to reconstruct the complete shape of a soft robot [29]. Therefore, we use this approach to capture ground truth information for soft actuators with different types of deformation.

3) Machine learning: Due to the highly nonlinear deformation presented on soft bodies, it is difficult to build an accurate analytical sensing model for soft robots. Simplified analytical models can only be applied to a specific type of design and thus lack of generality. Machine learning methods, particularly artificial neural networks, have proved to be a powerful tool to learn these nonlinearities while being applicable to a wide range of designs. Feedforward neural networks (FNNs) have been used to learn the kinematics of soft robots [24], [30] and to characterize various types of soft sensors [22], [25], [28], [29], [31]. When sequential data is collected, a recurrent neural network (RNN) or long short-term memory (LSTM) network can be used to include time-variant effects such as hysteresis in the sensing model [7], [8], [16], [32]. As a powerful tool when working with camera data as sensor input, a convolutional neural network (CNN) has been employed in combination with an LSTM to calibrate a soft tactile sensor for detecting the hardness of objects [33]. We employ neural networks in our learning process to establish the mapping between the signals from sensors and the shape parameters that are extracted from the captured positions of markers.

B. Our Approach

Our approach endows soft pneumatic actuators with the sensing capability for real-time 3D shape reconstruction through four steps (see Fig. 1):

1) Embedding optical sensors and lamps into the air chambers of soft robots to translate deformations of the air chambers to the variation of light intensity;
2) Capturing the ground truth deformation of the soft robot using markers placed on the robot;
3) Extracting shape parameters that can represent deformation more compactly from the positions of markers;

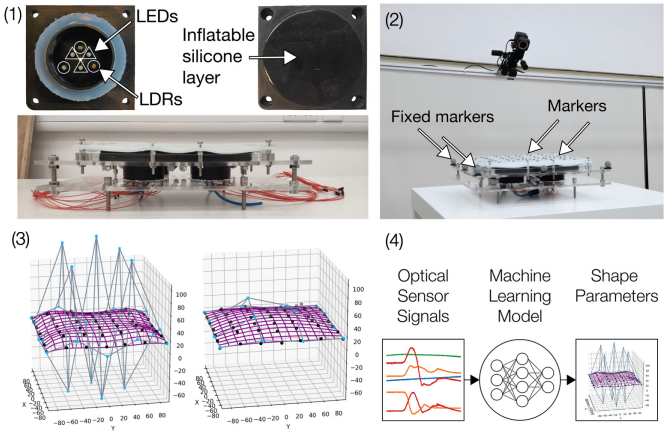

Fig. 1. Overview of our approach for enabling the sensing capability of 3D shape on soft robots in four steps: (1) sensor integration, (2) data collection, (3) shape parameterization, and (4) learning the mapping.

4) Learning the mapping between the signals captured on sensors and the corresponding deformation represented by shape parameters.

To the best of our knowledge, this is the first work that provides a full pipeline for real time 3D reconstruction of pneumatic soft robots consisting of multiple interacting actuators. This was made possible due to the following technical contributions:

- Accurate proprioception method for pneumatic soft robots consisting of multiple interacting actuators undergoing 3D deformation;
- A method to efficiently reconstruct the three-dimensionally deformed overall shape by directly learning the mapping between the sensed signals and the shape parameters.

Due to the small number of sensors as well as the efficient mapping between the sensor readings and the shape parameters used for reconstruction, both the sensing and the reconstruction steps can run at 50 Hz on a consumer-level device.

Two vastly different robot designs – a robotic joint and a deformable membrane – were selected to demonstrate the flexibility of the proprioception method as well as the shape parameterization. The robotic joint is composed of three interacting bellows that can extend and bend to a great extent without presenting large material strains. As the bellows are connected to the same rigid body as end-effector, the deformation can be parameterized as a transformation matrix to compute the forward kinematics easily. On the other hand, the deformable membrane is composed of four modules that inflate the stretchable silicone layer to form a 3D freeform surface. Real-time reconstruction of free-form surfaces is challenging. In this work, shape of the deformable membrane is parameterized by the control points of a Bézier surface.

II. Sensing Deformation on Soft Actuators

This section explains the importance of using multiple sensors to capture the deformation of pneumatic actuators on soft robots. Deformation of an actuator with one DOF can often

be captured by a single sensor. However, the signals captured by a single sensor cannot distinguish the configurations of deformation in multi-DOF actuators. Attempts have been made to increase the number of signals that can be captured by using a camera instead of single (optical) sensors (ref. [16], [17], [18], [19], [20]). For example, if images are taken at the resolution of 1280×720, this method can capture up to $1280 \times 720 \times 3 = 2,764,800$ different signals. However, in practice, the number of sensors required for capturing 3D deformation is much smaller than this as redundancy exists in sensing and computation. Besides the excessive computing time, another downside of camera-based sensing is the difficulty of integrating it into a narrow space, which is quite common in many soft actuators. In our approach, we place LEDs and LDRs inside each air chamber to capture the deformation inside a chamber. The signals captured in all chambers are later fused to reconstruct a 3D shape of the soft robot driven by these chambers.

It is important to capture the deformation on each chamber. As shown in the experiment of Fig. 2, the 3D transformation can already be well reconstructed even if only one bellow (i.e., the air chamber) is equipped with sensors. However, as multiple configurations exist for which a single sensor gives the same reading, a chamber should have multiple sensors to make a distinction between these configurations – see the difference between blue (only one LDR inside the bellow) and light red (with four LDRs inside the bellow). As the ends of the three bellows are connected to the same rigid frames, their deformations are somewhat coupled. Therefore, the accuracy obtained using four LDRs in one bellow already approaches that of using four LDRs in every bellow (i.e., $4 \times 3 = 12$ LDRs in total). However, this is not the case for many other soft robots with multiple actuators, such as the deformable membrane shown in Figs.1 and 4.

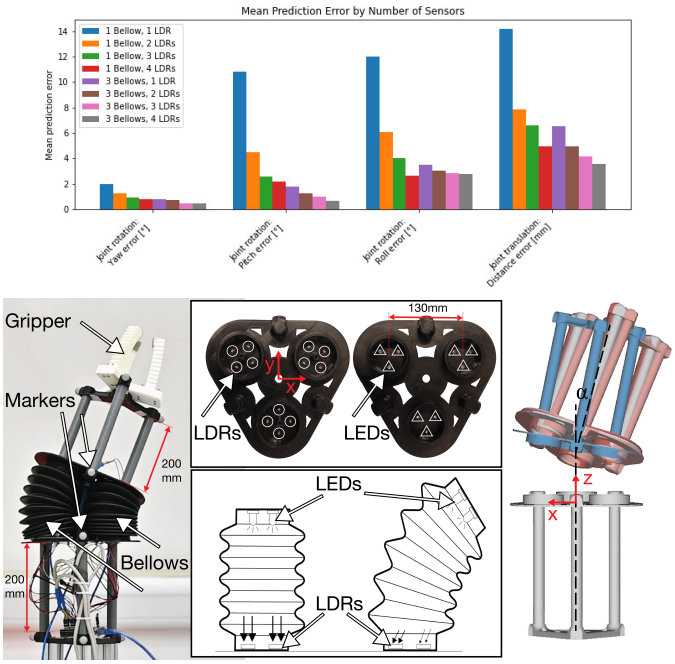

Fig. 2. (Top row) The mean prediction errors generated by using different numbers of light-dependent resistors (LDRs) inside either only one bellow or inside all three bellows. (Bottom row) The predicted transformation is already highly accurate when using four LDRs in one bellow (light red). For the purpose of comparison, the predictions by using only one LDR in one bellow (blue) and four LDRs in all three bellows (gray) are also given. The ground truth transformation is calculated from markers located on the robot by using a motion capture system, and displayed in dark red. The layout of LDRs and light-emitting diodes (LEDs) and the illustration of their working principle are also given in the bottom row.

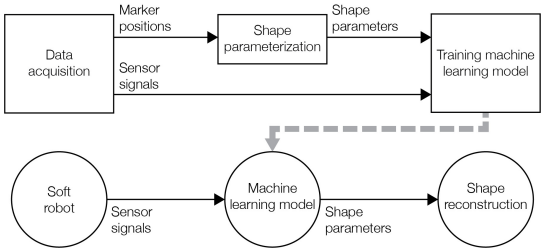

Fig. 3. (Top) The framework diagram for training the neural network and (bottom) the pipeline for real-time reconstruction.

III. Soft Robot Realization

In this section, we present the realization of our sensing and reconstruction method on two different designs of soft robots. Methods for data acquisition and shape parameterization are also introduced. Lastly, we discuss the feasibility of using different machine learning approaches. The process from data acquisition to training the machine learning model is described by the framework diagram shown in Fig. 3, which also presents the pipeline for real-time reconstruction.

A. Two Soft Robots

1) Soft continuum joint: The design of a soft continuum joint is indicated in Fig. 2. The soft continuum joint is composed of three inflatable bellows, the top and bottom of which are attached to two rigid frames. The centers of these frames are connected by a cable that constrains the longitudinal expansion of the bellows such that a multi-directional bending motion can be generated upon inflating the bellows. The maximum bending angle α (see Fig. 2) is at least 26 degrees in all directions and the operating pressure is in the range of [0, 10] kPa. The top and bottom frame of the joint are fabricated by using fused deposition modeling (FDM) with black polyactic acid (PLA) filaments. The leads of the LEDs and LDRs are fed through small holes in the frames and sealed with epoxy glue. The bellows are off-the-shelf Freudenberg V6-00400 bellows, which are sealed around the cylindrical parts of the frame using cable ties. In each bellow, four LDRs are mounted on the bottom frame to measure the light intensity inside the bellow. This light is generated by three LEDs mounted on the top frame of each bellow. Deformations of the bellows result in variation of light intensity that is sensed by the LDRs. The change of sensed light intensity is indicated by the changed lengths of the black arrows illustrated in the inset of Fig. 2. This information can be used to determine the deformed shape of a bellow. As different external forces are applied to the joint when the gripper mounted on top of the arm holds different objects, rotation and translation of the

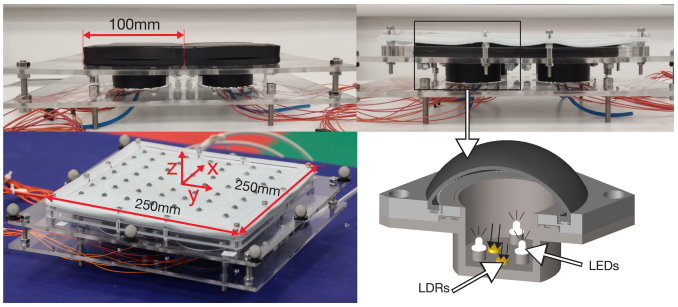

Fig. 4. The hardware setup of the deformable membrane and its main dimensions. An illustration of the inflated module and its inner layout is shown in the bottom right.

joint cannot be determined from the pressure of air inside the bellows. Sensors are needed to determine the rotation and translation of the joint based on the shape variation of the bellows. Due to the application of machine learning, an accurate mapping between the sensor signals and soft robot shape can be learned regardless of variations in the sensors or their placement.

2) Soft deformable membrane: The design of a deformable membrane is as shown in Fig. 4. This hardware setup is composed of four chamber modules that can be inflated separately. The bottom of each module is rigid and mounted with three LEDs and three LDRs. The chamber is sealed by a lid with a thin inflatable silicone layer. The modules have been fabricated using a combination of FDM and silicone casting. A mechanical interlocking structure, as proposed by Rossing et al. [34], is used to create an airtight bond between the 3D-printed part and the silicone. The silicone used is *Smooth-On Dragonskin* with a shore hardness of $30A$ colored with black silicone pigment. The filament used is black PLA. The materials were selected for their opacity in order to eliminate the influence of external lighting conditions on the sensor readings. When the chamber of a module is pressurized, the silicone layer inflates. This inflation results in a change in reflection and traveling distance of the light emitted by the LEDs, which is sensed by the LDRs. This information can be used to determine the shape of the inflated silicone. Four modules are mounted on a frame in a 2×2 layout and covered by a thin layer of silicone to create a smooth deformable membrane. The operating pressure is in the range of $[0, 15\mathrm{kPa}]$. The modules can be inflated to a height of up to $40\mathrm{mm}$. Note that as all four inflatable modules interact with the silicone layer and therefore are coupled, the shape of each module cannot be determined from the air pressure of each chamber. This effect is amplified by the highly non-linear material behavior of the silicone. Therefore, sensors are essential to determine the shape of the membrane.

B. Data Acquisition

This subsection introduces the method of generating the dataset for training.

1) Setup for data acquisition: A motion capturing system of Vicon was used to capture a number of strategically placed markers on the soft robots. For the soft continuum joint, markers were placed at the top and the bottom frame of the joint (see Fig. 2). For the soft deformable membrane, a layout of 7×7 markers was placed on top of the membrane. Additional markers were placed on the rigid frame as reference points for sensing its orientation. These markers are illustrated in Figs. 1 and 5. Upon data collection, the positions of markers were collected at a frequency of 100 Hz, whereas data of all 12 LDRs was collected at a frequency of 1000 Hz. The data was synchronized using the Vicon Lock Sync Box.

2) Sampling strategy: A good sampling scheme that spans the robot's workspace as well as a wide range of external loads was found crucial to prevent overfitting in data-driven learning. For the soft continuum joint, a range of weights were added on top of the actuator to enable accurate predictions when different external loads were applied to the joint. The weights held by the gripper on top of the arm varied from 0 to $500\mathrm{g}$ in steps of $50\mathrm{g}$. A total of $242,131$ samples were collected in $40\mathrm{m}21\mathrm{s}$. Note that each sample refers to a collection of the markers' positions. The data collection was divided into three batches. These batches were collected at different times of a day and with an altered orientation and position of the soft robot in the room to guarantee independence of external lighting conditions and the calibration of the motion capturing system. For the deformable membrane, the actuation sequence was varied to ensure that samples can span the entire working space. The data was collected in two batches with varying positions and orientations of the robot as well as varying lighting conditions. A total of $44,403$ samples were collected in $7\mathrm{m}24\mathrm{s}$ for the soft deformable membrane.

3) Data Preparation: Before further processing of the data, the captured marker positions were converted into a more convenient system aligned with the robots. The origin of the soft continuum joint was selected as the center of the bottom triangle of the joint. The z-axis was aligned with the triangle's normal pointing upwards, the y-axis pointed from origin towards one of the markers, and the x-axis was then defined as orthogonal to these two axes (see Fig. 2). For the soft deformable membrane, the centroid of the fixed markers on the frame was selected as the origin. The axes were defined such that the x- and y-axes aligned with the frame's boundary and z-axis pointed upwards.

C. Shape Parameterization

The most intuitive way to present the shape of a deformed soft robot is to describe it by the predicted locations of markers [22]. However, this approach is redundant in many scenarios. Two shape parameterizations are introduced below for the hardware setups employed in our work, which provides a more compact and effective way to reconstruct the shape of deformed soft robots.

1) Soft continuum joint: A parameterization with physical meaning is demonstrated for this hardware setup. The collected marker positions are converted to a rigid transformation represented by a rotation matrix $\mathbf{R}$ together with a translation vector $\mathbf{T}$, which describe the rotation and translation from the bottom triangle of the joint to the top triangle of the joint. For a set of points (i.e., markers) on the bottom triangle denoted as

$\{\mathbf{m}_i\}$ and the corresponding set of points on the top triangle as $\{\mathbf{d}_i\}$, the mapping between them can be described as

$$\mathbf{d}_i = \mathbf{R}\mathbf{m}_i + \mathbf{T} + \mathbf{v}_i \tag{1}$$

where $\mathbf{v}_i$ is a noise vector to incorporate the errors of marker placement and measurement. The best solution of $\mathbf{R}$ and $\mathbf{T}$ can then be determined by the unit-quaternion approach in the sense of minimizing a least-squares error (ref. [35]). The set of $(\mathbf{R}, \mathbf{T})$ determined from motion capture are used as samples for training and testing.

2) Soft deformable membrane: For the soft deformable membrane, a parameterization based on Bézier surfaces is conducted to represent its shape more compactly than by the positions of markers on the robot. The positions of 7×7 ($N = 49$) markers are used to provide raw data for presenting the shape of a deformed membrane. A surface fitting process is conducted to generate the control points of a Bézier surface patch for describing the shape. In general, a Bézier surface maps parameters (u, v) to surface point coordinate $\mathbf{p} \in \Re^3$ as

$$\mathbf{p}(u, v) = \sum_{i=0}^{m} \sum_{j=0}^{n} B_{i,m}(u) B_{j,n}(v) \mathbf{c}_{i,j} \tag{2}$$

where $\{\mathbf{c}_{i,j}\}$ are control points of the surface and $B_{i,m}(u)$ and $B_{j,n}(v)$ are Bernstein basis polynomials defined as

$$B_{i,m}(u) = \binom{m}{i} u^i (1-u)^{m-i}. \tag{3}$$

For this hardware setup, the positions of markers can be captured by the motion capture system. For a marker with position $\mathbf{p}_k$, we can determine its parameters (u_k, v_k) by the marker's planar coordinate when the membrane is flat – that is, before pumping air into the chambers. The control points can be determined by minimizing the following energy, which measures the square distances between the real coordinates of markers (captured by cameras) and the positions obtained by surface description

$$E = \sum_{k=0}^{N-1} (\mathbf{p}_k - \sum_{i=0}^{m} \sum_{j=0}^{n} B_{i,m}(u_k) B_{j,n}(v_k) \mathbf{c}_{i,j})^2. \tag{4}$$

With the help of Bézier surface fitting, the deformable membrane could be expressed as the linear combination of several control points, thus removing the redundant information embedded in the marker positions. Moreover, this compact representation is more robust to noises and outliers. The accuracy of the shape representation is dependent on the number of control points of the Bézier surface. As the Bézier surface is a special case of B-spline surface, the extension to a B-spline surface is also straightforward. However, increasing the number of control points means that more information needs to be generated from the sensed signals. As a result, a more complex machine learning model is needed, and such a model generally must also be fed by more training samples. As the dataset is obtained through physical experiments, the collection of additional samples is time-consuming and thus expensive. Figure 5 displays a comparison of the fitting of a Bézier surface with 16, 25, and 36 control points. It can be seen that a Bézier surface with 5×5 control points can already describe the deformable membrane with accuracy at a satisfactory level.

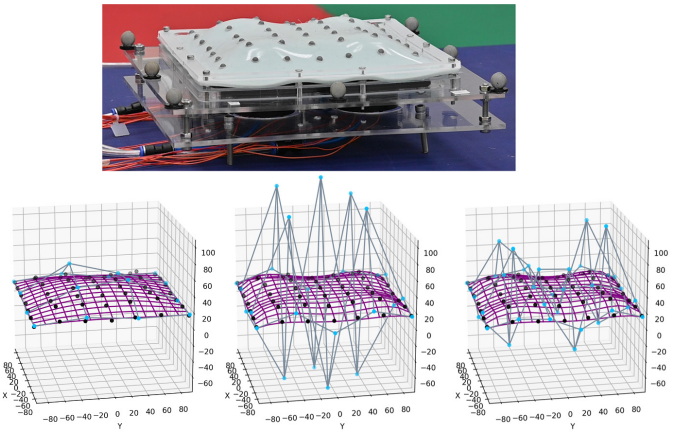

Fig. 5. Surface fitting for a deformed surface (top row) with 49 markers' positions determined by a motion capture system. The results by using 4×4, 5×5, and 6×6 control points are given from left to right (bottom row). The black points indicate the measured coordinates of markers, the blue points present the control points obtained by surface fitting and the fitted Bézier surfaces are visualized as the purple grids.

D. Machine Learning

Machine learning is applied to learn the relationship between the sensor data and the shape-oriented parameters. We studied different learning models to determine the best model for different hardware setups. For this purpose, accuracy was tested on different trained models, including an LSTM network, an FNN, a support vector regression (SVR), and a multivariate linear regression (MVLR). The network design of these models is presented below.

- The LSTM network has a hidden layer of 50 neurons with $\tanh(\cdot)$ as the activation function. In the output layer, a linear function is used for learning the translation and the control points of the Bézier surface, while $\tanh(\cdot)$ is employed for learning the rotation matrix.
- For the learning model by FNN, we also use a hidden layer of 50 neurons with sigmoid as the activation function. The output layer is designed identical to the LSTM network.
- For SVR, we chose standard radial basis functions (RBF) as kernels and used 1.0 as the C-parameter for regularization.
- An ordinary least squares multivariate linear regression is used for MVLR.

For the soft deformable membrane, we obtained the datasets for training, validation, and testing from the readings from 12 sensors in 10 subsequent time-steps at 1000 Hz, resulting in $12 \times 10 = 120$ readings as input for each prediction. Positions of markers were captured by cameras and converted into control points of a Bézier surface – specifically, we generated different control polygons with 4×4, 5×5, and 6×6 to explore the best result. To verify the generality of a learning model's performance, the actuation sequence that was used to generate the dataset of the test must be different from the actuation sequence used to generate the training dataset. For the soft continuum joint, the datasets were also obtained from the readings from 12 sensors and the captured positions of markers in 10 subsequent time-steps at 1000 Hz, again resulting in

TABLE I
DATASETS FOR MACHINE LEARNING

Hardware Setups	# Samples in Different Datasets		
	Training	Validation	Test
Continuum Joint	168, 251	50, 510	23, 370
Deformable Membrane	21, 396	11, 503	11, 504

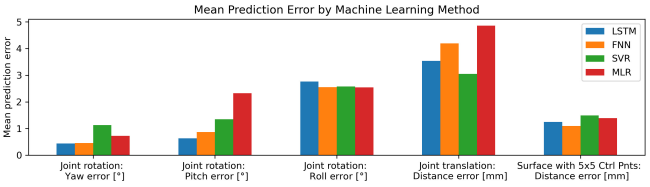

Fig. 6. Comparison of the mean prediction errors by using different learning models for the soft continuum joint and the soft deformable membrane.

$12 \times 10 = 120$ readings as input for each prediction. The positions of markers were converted into a rotation matrix and a translation vector to form a sample. The performance of learning models was evaluated on the dataset captured while external loads were applied. Note that these specific external loads were not applied while generating training data so that the generality of a learning model is well verified. The total numbers of samples in different datasets and the comparison of mean prediction errors are given in Table I.

IV. RESULTS

This section presents the experimental results of applying our approach on the two hardware setups – the soft continuum joint and the soft deformable membrane. Quantitative analysis was conducted to verify the performance of our method. The performance of different machine learning models is compared and displayed in Fig. 6 for the soft continuum joint and the soft deformable membrane. It is found that both LSTM and FNN perform well in general. However, we did not find clear indicators to predict which of these two networks will perform better on a specific shape parameterization.

A. Soft Continuum Joint

To provide a more meaningful interpretation of the errors in the rotation matrix, the prediction errors of a rotation matrix are translated to Tait-Bryan Euler angles following the $z-$, $y'-$, and $x''-$-convention (intrinsic rotations) – referred to as yaw, pitch, and roll respectively. The best performance was achieved using the LSTM with mean prediction errors as 0.44, 0.63, and 2.76 degrees in yaw, pitch, and roll, respectively. Prediction error of the translation vector is evaluated by the error vector's magnitude. According to the evaluation of the test dataset, SVR gives the smallest error as 3.05 mm. LSTM's error is 3.53 mm, which is comparable to SVR. Therefore, by combining rotation and translation, the LSTM learning model provides the best performance. Mean prediction errors and their distribution are shown in Fig. 7.

A side-by-side comparison of the reconstructed joint and the real joint position for a time sequence of 16 seconds is shown in Fig. 8 and also the supplementary video. This

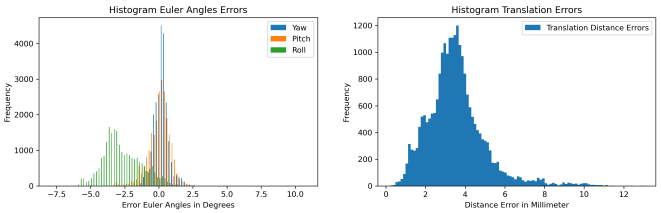

Fig. 7. Histograms of the prediction errors for the rotation (left) and the translation (right) of the soft continuum joint, where the prediction is generated by the LSTM network.

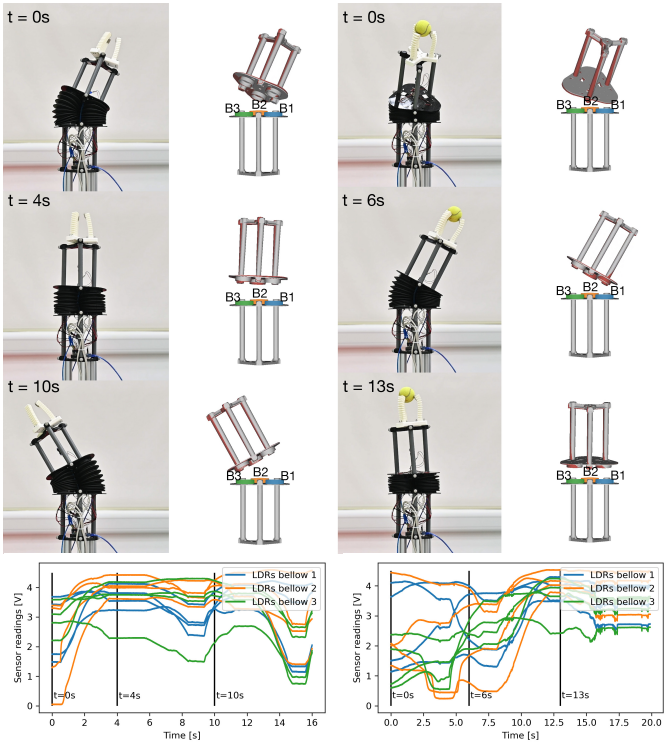

Fig. 8. Comparison of the rotation and translation predicted by the LSTM network on the continuum joint and the actual rotation and translation (obtained from motion capture) for a sequence without external load (left) and with external load (right). The transformation obtained from motion capture is displayed in dark red, while the reconstructed transformation from LSTM prediction is rendered in gray. LDRs sensor readings in different modules throughout the time sequences are shown at the bottom. Bellows and their corresponding set of LDR sensor readings are visualized in matching colors.

reconstruction is based on the predictions obtained from the LSTM model, which demonstrate the capability of accurate prediction regardless of the external load.

A prediction for the rotation and translation can be generated within 4 ms on a consumer-level device (i.e., a laptop PC with 2.3GHz CPU + 16GB RAM), whereas the calculation of the forward kinematics is very fast. In practice, the sensor readings can be obtained at the rate of 1000 Hz, and each prediction is made by using readings from 10 time-steps. Therefore, we can make a prediction in a single-thread computation (see the bottom row of Fig. 3) every 14 ms, which makes it possible to run the reconstruction in real-time (at the rate of 50 to 70 Hz). The speed of visualizing deformed 3D models as shown in Fig. 8 depends on the mesh density.

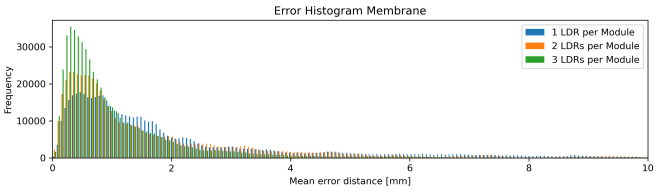

Distance Errors	1 LDR	2 LDRs	3 LDRs
Mean Values	2.21mm	1.79mm	1.18mm
Standard Deviation	2.44mm	2.06mm	1.39mm

Fig. 9. Histogram showing the distribution of the distance errors between the real and the predicted marker positions for the samples in the test dataset when using different numbers of LDRs in each module.

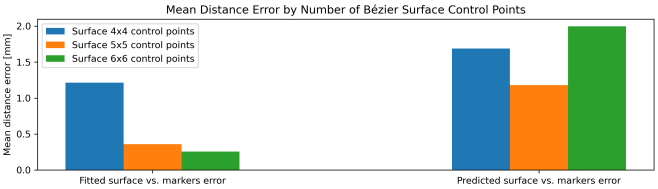

Fig. 10. Comparison of the mean distance error for the fitted surface vs. the captured markers, and the predicted surface vs. the captured markers on Bézier surfaces with different numbers of control points.

B. Soft Deformable Membrane

The prediction error of the soft deformable membrane is indicated on the right side of Fig.6. For each marker, its uv-parameters can used to generate the marker's position on the predicted surface. The distance between the real position of a marker (obtained from motion capture) and its predicted position is employed as a metric to evaluate the error. When comparing the mean errors, FNN gives the best result with 1.18 mm as the mean of distance errors. An error histogram is given in Fig. 9. It is also interesting to study the influence of different numbers of sensors. Therefore, we also generated results by the test dataset using only two LDRs and one LDR per module. Their corresponding error histograms are also shown in Fig. 9. It can be observed that the mean distance error by using only one LDR within each module is nearly twice the error when using three LDRs.

We also studied the errors by using different numbers of control points for Bézier fitting. The errors were measured as the distances between the positions of markers and their corresponding points on the resultant surface of fitting. It is obvious that more control points lead to less fitting error (see the left side of Fig. 10). However, the error of a surface (with 6×6 control points) predicted from sensor readings can be larger than the error on a surface with 5×5 control points (see the right of Fig. 10). The reason is twofold. First of all, the surface fitting error of 5×5 is already very close to the error of 6×6. Secondly, the information from 12 sensors is not sufficient to predict 36 control points. Therefore, we used 5×5 control points to represent and reconstruct the soft deformable membrane.

A visual comparison of the physically deformed membrane and the reconstructed surface over a period of 29 seconds can be found in Fig. 11 and also the supplementary video. The surface is predicted by FNN from the light intensities captured by LDRs in each module. The distance errors between the surface predicted from sensor readings and the surface generated by fitting camera captured positions of markers are visualized as color maps.

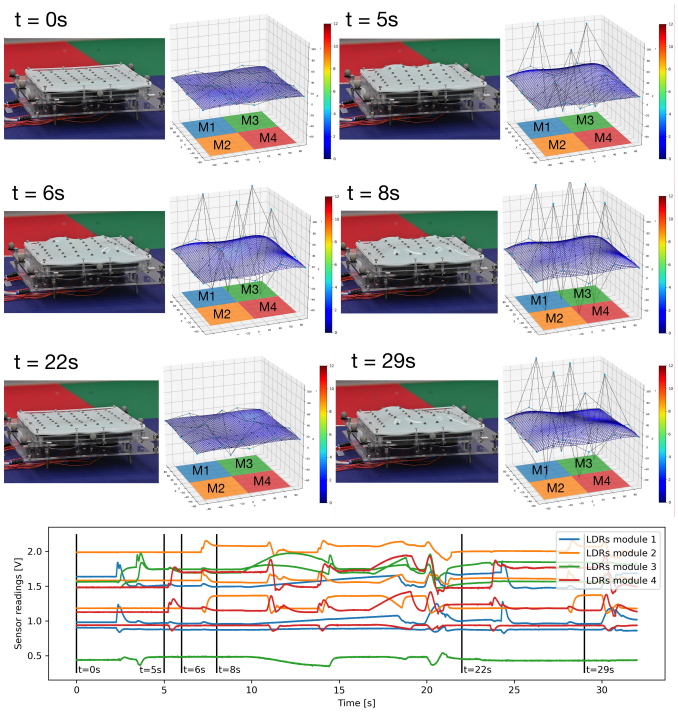

Fig. 11. Visual comparison of the FNN predicted surface represented by 5×5 control points and the physically deformed soft membrane during a time sequence of 29 seconds. The positions of markers obtained from motion capture are displayed in black dots, while their corresponding points on the predicted surface are connected by red line segments. The errors between the predicted surface and the captured surface (by fitting camera-captured positions of markers) are visualized as color maps. The sensor readings of the LDRs within the different modules throughout the time sequence are shown in the bottom graph. Modules and their corresponding set of LDR sensor readings are indicated in matching colors.

Prediction of the control points from sensor readings can be generated within 1 ms on a consumer-level device. Again we made a prediction by using the readings from 10 time-steps, which is captured at the rate of 1000 Hz. The speed of visualization as shown in Fig. 11, strongly depends on the density of the grid – for example, a visualization with a 30×30 grid can be generated within 6ms using a C++ implementation. Incorporating all these computations, our system can be operated in real-time at the rate of more than 50 Hz.

V. Conclusion

In this paper, we presented a method to sense and reconstruct 3D deformation on pneumatic soft robots composed of multiple actuators. Our method is based on integrating multiple low-cost sensors inside the chambers of pneumatic actuators and then using machine learning to fuse the captured signals into shape parameters of the soft robots. These shape parameters can be used to efficiently reconstruct the 3D shape of the soft robot. The sensing and shape prediction pipeline can run at 50 Hz in real time on a consumer-level device.

This is an important step towards the development of more advanced closed-loop control for soft robots.

In this work, LDRs were chosen to capture the changes in light conditions. It should be noted that the resistivity of these semiconductors changes with temperature and humidity. In our experiments, this did not raise any issues when testing under mildly varying (room temperature) conditions. If a robot is required to operate under severe temperature changes, it is recommended to replace the LDRs with photodiodes as our previous work [22] or to add a temperature sensor for further calibration. Future research could investigate the use of transfer learning to reduce the required number of new training samples when a minor modification is applied to a design. Lastly, the simulation of light variation inside the air chambers could be a promising direction for optimizing the placement of the optical sensors and the light sources inside air chambers. This simulation could also be used for integrating other effective signal generators, such as color patterns [21], to further increase the accuracy of proprioception.

REFERENCES

[1] K. Elgeneidy, N. Lohse, and M. Jackson, "Bending angle prediction and control of soft pneumatic actuators with embedded flex sensors – a data-driven approach," *Mechatronics*, vol. 50, pp. 234 – 247, 2018.

[2] H. Zhao, R. Huang, and R. F. Shepherd, "Curvature control of soft orthotics via low cost solid-state optics," in *2016 IEEE International Conference on Robotics and Automation (ICRA)*, 2016, pp. 4008–4013.

[3] J. Morrow, H. Shin, C. Phillips-Grafflin, S. Jang, J. Torrey, R. Larkins, S. Dang, Y. Park, and D. Berenson, "Improving soft pneumatic actuator fingers through integration of soft sensors, position and force control, and rigid fingernails," in *2016 IEEE International Conference on Robotics and Automation (ICRA)*, May 2016, pp. 5024–5031.

[4] K. Elgeneidy, G. Neumann, M. Jackson, and N. Lohse, "Directly printable flexible strain sensors for bending and contact feedback of soft actuators," *Frontiers in Robotics and AI*, vol. 5, p. 2, 2018.

[5] Y. Yang and Y. Chen, "Innovative design of embedded pressure and position sensors for soft actuators," *IEEE Robotics and Automation Letters*, vol. 3, no. 2, pp. 656–663, 2018.

[6] R. L. Truby, M. Wehner, A. K. Grosskopf, D. M. Vogt, S. G. M. Uzel, R. J. Wood, and J. A. Lewis, "Soft somatosensitive actuators via embedded 3D printing," *Advanced Materials*, vol. 30, no. 15, p. 1706383, 2018.

[7] T. G. Thuruthel, B. Shih, C. Laschi, and M. T. Tolley, "Soft robot perception using embedded soft sensors and recurrent neural networks," *Science Robotics*, vol. 4, no. 26, 2019.

[8] R. L. Truby, C. D. Santina, and D. Rus, "Distributed proprioception of 3D configuration in soft, sensorized robots via deep learning," *IEEE Robotics and Automation Letters*, vol. 5, no. 2, pp. 3299–3306, 2020.

[9] S. Ozel, E. H. Skorina, M. Luo, W. Tao, F. Chen, Yixiao Pan, and C. D. Onal, "A composite soft bending actuation module with integrated curvature sensing," in *2016 IEEE International Conference on Robotics and Automation (ICRA)*, May 2016, pp. 4963–4968.

[10] W. Felt, M. Suen, and C. D. Remy, "Sensing the motion of bellows through changes in mutual inductance," in *IEEE/RSJ International Conference on Intelligent Robots and Systems (IROS)*, 2016, pp. 5252–5257.

[11] W. Felt, M. J. Telleria, T. F. Allen, G. Hein, J. B. Pompa, K. Albert, and C. D. Remy, "An inductance-based sensing system for bellows-driven continuum joints in soft robots," *Auton. Robots*, vol. 43, no. 2, pp. 435–448, Feb. 2019.

[12] H. Bai, S. Li, J. Barreiros, Y. Tu, C. R. Pollock, and R. F. Shepherd, "Stretchable distributed fiber-optic sensors," *Science*, vol. 370, no. 6518, pp. 848–852, 2020.

[13] S. Sareh, Y. Noh, M. Li, T. Ranzani, H. Liu, and K. Althoefer, "Macrobend optical sensing for pose measurement in soft robot arms," *Smart Materials and Structures*, vol. 24, no. 12, p. 125024, Nov. 2015.

[14] Teichert Systemtechnik GmbH. (2019) Innovative cable-like-shape-sensor. [Online]. Available: http://www.tst-inno.de/cable-like-shape-sensor/?lang=en

[15] R. Wang, S. Wang, E. Xiao, K. Jindal, W. Yuan, and C. Feng, "Real-time soft robot 3D proprioception via deep vision-based sensing," *CoRR*, vol. abs/1904.03820, 2019. [Online]. Available: http://arxiv.org/abs/1904.03820

[16] G. Soter, H. Hauser, A. Conn, J. Rossiter, and K. Nakajima, "Shape reconstruction of CCD camera-based soft tactile sensors," in *IEEE/RSJ International Conference on Intelligent Robots and Systems*, 2020.

[17] B. Ward-Cherrier, N. Pestell, L. Cramphorn, B. Winstone, M. E. Giannaccini, J. Rossiter, and N. F. Lepora, "The TacTip family: Soft optical tactile sensors with 3D-printed biomimetic morphologies," *Soft Robotics*, vol. 5, no. 2, pp. 216–227, 2018.

[18] X. Lin, L. Willemet, A. Bailleul, and M. Wiertlewski, "Curvature sensing with a spherical tactile sensor using the color-interference of a marker array," in *2020 IEEE International Conference on Robotics and Automation (ICRA)*, 2020.

[19] W. Yuan, S. Dong, and E. Adelson, "GelSight: High-resolution robot tactile sensors for estimating geometry and force," *Sensors*, vol. 17, no. 12, p. 2762, Nov. 2017.

[20] P. Werner, M. Hofer, C. Sferrazza, and R. D'Andrea, "Vision-based proprioceptive sensing: Tip position estimation for a soft inflatable bellow actuator," in *2020 IEEE/RSJ International Conference on Intelligent Robots and Systems (IROS)*, Oct. 2020.

[21] R. B. N. Scharff, R. M. Doornbusch, X. L. Klootwijk, A. A. Doshi, E. L. Doubrovski, J. Wu, J. M. P. Geraedts, and C. C. L. Wang, "Color-based sensing of bending deformation on soft robots," in *IEEE International Conf. on Robotics and Automation (ICRA)*, 2018, pp. 4181–4187.

[22] R. B. N. Scharff, R. M. Doornbusch, E. L. Doubrovski, J. Wu, J. M. P. Geraedts, and C. C. L. Wang, "Color-based proprioception of soft actuators interacting with objects," *IEEE/ASME Transactions on Mechatronics*, vol. 24, no. 5, pp. 1964–1973, 2019.

[23] A. Buso, R. B. N. Scharff, E. L. Doubrovski, J. Wu, C. C. L. Wang, and P. Vink, "Soft robotic module for sensing and controlling contact force," in *IEEE International Conf. on Soft Robotics*, 2020, pp. 70–75.

[24] M. Giorelli, F. Renda, M. Calisti, A. Arienti, G. Ferri, and C. Laschi, "Neural network and Jacobian method for solving the inverse statics of a cable-driven soft arm with nonconstant curvature," *IEEE Transactions on Robotics*, vol. 31, no. 4, pp. 823–834, Aug. 2015.

[25] I. M. Van Meerbeek, C. M. De Sa, and R. F. Shepherd, "Soft optoelectronic sensory foams with proprioception," *Science Robotics*, vol. 3, no. 24, 2018.

[26] R. Xu, A. Asadian, A. S. Naidu, and R. V. Patel, "Position control of concentric-tube continuum robots using a modified Jacobian-based approach," in *ICRA*. IEEE, 2013, pp. 5813–5818.

[27] M. Bächer, B. Hepp, F. Pece, P. G. Kry, B. Bickel, B. Thomaszewski, and O. Hilliges, "DefSense: Computational design of customized deformable input devices," in *Proceedings of the 2016 CHI Conference on Human Factors in Computing Systems*. ACM, 2016, pp. 3806–3816.

[28] T. L. T. Lun, K. Wang, J. D. L. Ho, K. Lee, K. Y. Sze, and K. Kwok, "Real-time surface shape sensing for soft and flexible structures using fiber bragg gratings," *IEEE Robotics and Automation Letters*, vol. 4, no. 2, pp. 1454–1461, Apr. 2019.

[29] O. Glauser, D. Panozzo, O. Hilliges, and O. Sorkine-Hornung, "Deformation capture via soft and stretchable sensor arrays," *ACM Trans. Graph.*, vol. 38, no. 2, pp. 16:1–16:16, Mar. 2019.

[30] G. Runge, M. Wiese, and A. Raatz, "FEM-based training of artificial neural networks for modular soft robots," in *IEEE International Conference on Robotics and Biomimetics*, Dec. 2017, pp. 385–392.

[31] C. Sferrazza and R. D'Andrea, "Transfer learning for vision-based tactile sensing," *CoRR*, vol. abs/1812.03163, 2018.

[32] S. Han, T. Kim, D. Kim, Y. Park, and S. Jo, "Use of deep learning for characterization of microfluidic soft sensors," *IEEE Robotics and Automation Letters*, vol. 3, no. 2, pp. 873–880, Apr. 2018.

[33] W. Yuan, C. Zhu, A. Owens, M. A. Srinivasan, and E. H. Adelson, "Shape-independent hardness estimation using deep learning and a GelSight tactile sensor," in *2017 IEEE International Conference on Robotics and Automation (ICRA)*, May 2017, pp. 951–958.

[34] L. Rossing, R. B. N. Scharff, B. Chömpff, C. C. L. Wang, and E. L. Doubrovski, "Bonding between silicones and thermoplastics using 3D printed mechanical interlocking," *Materials & Design*, vol. 186, p. 108254, 2020.

[35] D. W. Eggert, A. Lorusso, and R. B. Fisher, "Estimating 3-D rigid body transformations: a comparison of four major algorithms," *Machine Vision and Applications*, vol. 9, no. 5, pp. 272–290, 1997.

Rob B.N. Scharff is a postdoctoral researcher in the Bioinspired Soft Robotics group at the Instituto Italiano di Tecnologia, Italy. He received the BSc and MSc degrees at the faculty of Industrial Design Engineering, Delft University of Technology, the Netherlands, in 2012 and 2015 respectively. In 2021, he obtained a PhD degree at the Materializing Futures section at Delft University of Technology. His research focuses on soft robotics, with an emphasis on soft pneumatic actuators with proprioception, and digital manufacturing.

Guoxin Fang Guoxin Fang (S'17) received the B.S. degree in mechanical engineering from the Beijing Institute of Technology, Beijing, China, in 2016. He is currently working as a research assistant in the Department of Mechanical, Aerospace and Civil Engineering, The Univerity of Manchester, UK. He is also now pursuing his Ph.D. degree in advanced manufacturing at the Delft University of Technology, Delft, the Netherlands. His research focuses on computational design, digital fabrication, and robotics.

Yingjun Tian Yingjun Tian is a Ph.D. student in the Smart Manufacturing group at the Department of Mechanical, Aerospace and Civil Engineering, the University of Manchester. He received his Bachelor Degree of Engineering in Mechanical Engineering and Automation, University of Science and Technology of China, Hefei, China in 2019. His research focuses on closed-loop control of soft pneumatic robots.

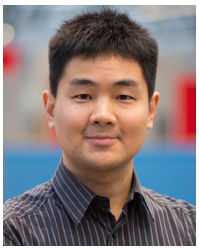

Jun Wu is an assistant professor at the Department of Sustainable Design Engineering, Delft University of Technology, the Netherlands. Before this, he was a Marie Curie postdoc fellow at the Department of Mechanical Engineering, Technical University of Denmark. He obtained a PhD in Computer Science in 2015 from TU Munich, Germany, and a PhD in Mechanical Engineering in 2012 from Beihang University, Beijing, China. His research is focused on computational design and digital fabrication, with an emphasis on topology optimization.

Jo M.P. Geraedts (1952) obtained a PhD in Physics at Radboud University, Nijmegen, the Netherlands. He joined Océ, today a Canon group company, in 1983 and worked at the development of digital print processes and workflow for document and industrial printing. From 2000 to 2013 he was manager of the Océ Industrial Design department and responsible for product, graphic, user interaction and usability design of all hardware and software developments in multidisciplinary teams worldwide. Jo Geraedts became in 2008 full Professor and chair Mechatronic Design at the faculty Industrial Design Engineering, Delft University of Technology, the Netherlands. His research focuses on 3D scanning, 3D multi-material printing, digital reproduction of Fine Arts, digital manufacturing and (soft) robotics.

Charlie C.L. Wang currently holds a Chair of Smart Manufacturing with the University of Manchester. Prior to this, he was a Chair of Advanced Manufacturing at Delft University of Technology and a Professor of Mechanical and Automation Engineering at the Chinese University of Hong Kong. He received his B.Eng. degree (1998) in mechatronics engineering from Huazhong University of Science and Technology and his M.Phil (2000) and Ph.D. (2002) degrees in mechanical engineering from Hong Kong University of Science and Technology (HKUST). Prof. Wang received a few awards from professional societies including the ASME CIE Excellence in Research Award (2016), the ISSMO/Springer Prize (2019), the Best Paper Award (2nd Place) of Solid and Physical Modeling (2019), the NAMRI/SME Outstanding Paper Award (2013), the Best Paper Awards of ASME CIE Conferences (twice in 2008 and 2001 respectively), the Prakash Krishnaswami CAPPD Best Paper Award of ASME CIE Conference (2011), and the ASME CIE Young Engineer Award (2009). He was elected Fellow of American Society of Mechanical Engineers (ASME) in 2013. His research interests include digital manufacturing, computational design, geometric computing and robotics.